

F61/62: Nuclear Magnetic Resonance

Yajie Liang and Leon Tschesche
supervised by: **Alena Harlenderova**

on Feburary 20th / 21th 2019

handed in as short report on: June 11, 2019

Abstract

This experiment has been performed as part of the advanced lab course for physics students (FP) at Heidelberg University.

The theoretical and experimental basics needed for the understanding of the conducted measurements is introduced and important concepts of nuclear magnetic resonance(NMR) are presented and discussed.

The characteristics of a NMR machine are analysed using data we recorded with the Bruker minispec p20 and the computer program LabView in the laboratory.

Furthermore we used Bruker minispec mq7.5 for getting 1d- and 2d-images of different subjects.

Lastly we present and discuss some applications of NMR in modern society.

Contents

1	Introduction	2
1.1	Basics of Nuclear Magnetic Resonance	2
1.2	Relaxation time	3
1.2.1	Spin-spin relaxation time T_2	3
1.2.2	Spin-lattice relaxation time T_1	4
1.3	Chemical shift	4
1.4	Imaging with NMR	5
2	Layout of the experiment	6
2.1	Relaxation Time and Chemical Shift	6
2.2	Imaging with NMR	7
3	Measurements and evaluation	7
3.1	Measurement of relaxation time	7
3.2	Chemical shift	8
3.3	Imaging with NMR	8
4	Discussion	10

List of Figures

1	Dephasing of transverse magnetization \vec{M}_\perp	4
2	Chemical Shift taken from [2]	4
3	One of the N Loops needed for 2D Imaging taken from [2]	6
4	The minispec p20, electronic unit on the left, magnetic unit on the right	6
5	Example of the used Labviews	7
6	The NMR analyzer and LabView for 2D imaging	7
7	NMR imaging 1D	9
8	NMR imaging 2D	9

1 Introduction

1.1 Basics of Nuclear Magnetic Resonance

Nuclear Magnetic Resonance (NMR), can only be observed for molecules with a non-zero magnetic dipole moment. For a given nuclei, whose spin \vec{J} is unequal to 0, its magnetic dipole moment can be calculated as

$$\vec{\mu} = \hbar\gamma\vec{J}. \quad (1)$$

where γ is the gyromagnetic factor. In this experiment we will look at exclusively protons, which have $\gamma_{proton} = 2.6752 \cdot 10^8 \text{ sec}^{-1} \text{ Tesla}^{-1}$.

The magnetization of N nuclei can be obtained by summing over all nuclei per unit volume

$$\vec{M} = \frac{1}{V} \sum_{i=1}^N \vec{\mu}_i \quad (2)$$

With the assumption of a weak field ($\mu B \ll kT$), which is the case in our experiment, it can be approximated by $\vec{M} \sim \frac{\vec{B}_0}{T}$ according to Curie's Law.

In general, the magnetization can have an arbitrary direction relative to external magnetic field. In the following we will decompose it into two components \vec{M}_{\parallel} (anti-)parallel and \vec{M}_{\perp} perpendicular to the external field. The magnetic dipole interacts with \vec{B}_0 and as a result the general state of magnetization will dissipate its excitation energy and reach the ground state, i.e. \vec{M}_{\parallel} , asymptotically on a characteristic time scale. The dissipated energy can be expressed by

$$\Delta E = -\vec{\mu} \cdot \vec{B}_0 \quad (3)$$

This interaction results in a torque and since \vec{B}_0 is parallel to \vec{M}_{\parallel} , the torque only acts on \vec{M}_{\perp} .

$$\vec{\tau} = \vec{M} \times \vec{B}_0 \quad (4)$$

Without a relaxation processes, the rate of change is given by

$$\frac{d\vec{M}_{\perp}}{dt} = -\gamma \vec{M}_{\perp} \times \vec{B}_0. \quad (5)$$

This differential equation can be solved by an ansatz $\vec{M} = M_{\perp}(\cos(\omega_L t), \sin(\omega_L t), 0)$ with ω_L being the Larmor frequency

$$\omega_L = \gamma B_0 \quad (6)$$

Now let's consider a ground state magnetization \vec{M} that is parallel to \vec{B}_0 and the z-axis. If we apply a sinusoidal voltage with frequency ω_{HF} to a coil which is coiled along the x-axis, it will result in a solenoidal magnetic field \vec{B}_1 which is perpendicular to \vec{B}_0 . This will lead to \vec{M} precessing around \vec{B}_1 . During a time interval Δt the angle α of the precession is then

$$\alpha = \gamma B_1 \Delta t. \quad (7)$$

If the time interval is chosen such that $\alpha = 90^\circ$, then \vec{M} is rotated into a perpendicular component \vec{M}_{\perp} along the y-axis. Such a pulse is called a 90° pulse. Similarly we define 180° pulse, which results in magnetization antiparallel to the static field \vec{B}_0 .

1.2 Relaxation time

Now we want to consider the relaxation process, which can be described with the Bloch equations. Here we introduce the rotating frame of the transverse magnetization, where the transverse magnetization is constant, if no relaxation processes take place. The Bloch equations assume that the time evolution is dominated by a restoring force which is proportional to the deflection from equilibrium

$$\frac{dM_{\perp}(t)}{dt} = -\frac{M_{\perp}(t)}{T_2} \quad (8)$$

$$\frac{dM_{\parallel}(t)}{dt} = -\frac{M_{\parallel}(t) - M_0}{T_1} \quad (9)$$

where T_2 is the spin-spin relaxation time, T_1 the spin-lattice relaxation time and M_0 the ground state magnetization.

In the laboratory system we can now write the equation (5) with (8) and (9) as

$$\frac{dM_{\perp}(t)}{dt} = -\frac{M_{\perp}(t)}{T_2} + \gamma(\vec{B} \times \vec{M})_{\perp} \quad (10)$$

$$\frac{dM_{\parallel}(t)}{dt} = -\frac{M_{\parallel}(t) - M_0}{T_1} + (\vec{B} \times \vec{M})_{\parallel} \quad (11)$$

1.2.1 Spin-spin relaxation time T_2

Spin-spin relaxation is caused by the interaction between different magnetic dipoles and it contributes to the transverse magnetization. This relaxation process is described by (10), which is solved by

$$M_{\perp}(t) = M_{\perp}^0 e^{-\frac{t}{T_2}}. \quad (12)$$

There are 2 methods for measuring T_2 using similar techniques. First let's look at the spin-echo method. We apply a 90° pulse at $t = 0$ to generate a transverse magnetization \vec{M}_{\perp} . We then wait for a time τ , after which we apply a 180° pulse and wait till $t = 2\tau$. At that time the magnetization should be transverse polarized again and we can measure the loss of amplitude. The described process is visualized in the following figure.

ω_a and ω_b are denoting 2 protons which experience different ω_L 's, which is caused by the inhomogeneities of the external \vec{B}_0 .

To measure the loss of amplitude we analyse the Fourier spectrum at time $t = 2\tau$ and integrate over the peak at the ω_L . If we repeat the process for different τ we will get a curve. This curve should follow (12), since the calculated amplitude is proportional to \vec{M}_{\perp} , and with the help of a fit we can extract the $T_{2,SE}$.

For the second method, the Carr-Purcell method, we also apply a 90° pulse at first and apply a 180° pulse at $t = \tau$. At $t = 2\tau$ the system should be in phase, but will dephase shortly after, same as in method one. We then apply another 180° at $t = 3\tau$ which will lead to a fully in phase system at $t = 4\tau$ again. This process can be continued for 180° at odd multiples of τ to get the system in phase at even τ . This process is a lot more precise for big τ in comparison to the spin-echo method, which gets inaccurate because of the molecular diffusion (the protons move away from their original position) and inhomogeneities in the field.

The measured amplitudes should still follow (12).

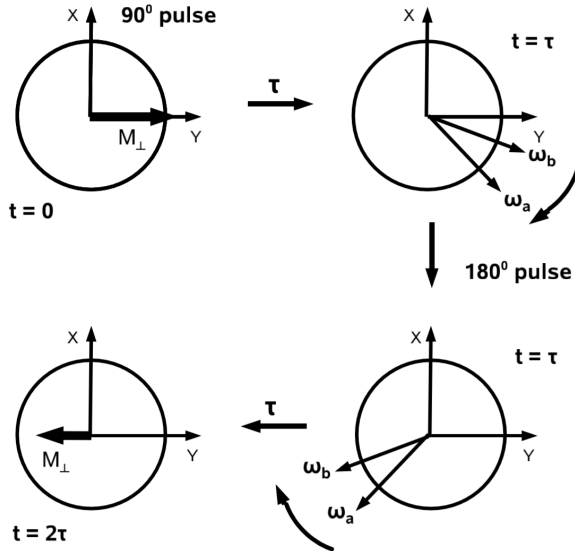


Figure 1: Dephasing of transverse magnetization \vec{M}_\perp
taken from [2]

1.2.2 Spin-lattice relaxation time T_1

Spin-lattice relaxation is caused by the interaction between the magnetic dipoles and the external magnetic field \vec{B}_0 and contributes to the parallel magnetization. This relaxation process is described by (11), which is solved by

$$M_{||}(t) = M_0(1 - 2e^{-\frac{t}{T_1}}). \quad (13)$$

We measure T_1 also with the spin-echo method. But this time we start at $t = 0$ with a 180° pulse and follow up after $t = \tau$ with a 90° pulse. We then measure the amplitude at $t = 2\tau$ for different τ and expect the resulting curve to follow (13).

1.3 Chemical shift

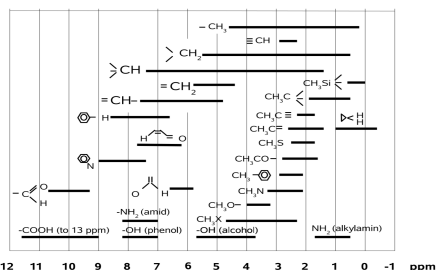


Figure 10: Chemical shifts δ_i of compounds relative to TMS.

(a) Chemical Shift δ_i

toluol	$\text{CH}_3-\text{C}_6\text{H}_5$
p-xylol	$\text{CH}_3-\text{C}_6\text{H}_3(\text{CH}_3)_2$
acetic acid	CH_3-COOH
fluoroacetone	$\text{FCH}_2-\text{CO}-\text{CH}_3$
fluoroacetonitrile	FCH_2-CN

Figure 11: Five substances for identification.

(b) Substances to be sorted

Figure 2: Chemical Shift taken from [2]

If a proton is bound by a molecule, it will experience a magnetic field that is weaker than the external magnetic field \vec{B}_0 because of the shielding effect of electrons. This leads to a modified resonance frequency ω_i for the proton. This frequency can be then used to identify unknown substances. To do so, it is easiest to compare it to a reference substance, which can be easily identified in a Fourier spectrum, since the whole frequency scale is dependent on \vec{B}_0 , i.e. a relative scale, and absolute frequency values can't be used. We are using Tetra-Methyl-Silan

(TMS), since its peak is always clearly visible and in our case always be the peak on the most left. With the help of ω_{TMS} one can define a chemical shift

$$\delta_i = \frac{\omega_{TMS} - \omega_i}{\omega_L} \quad (14)$$

for different molecular parts in reference to TMS as shown above in figure 2a. In this experiment we want to identify the substances in figure 2b from 5 different probes.

1.4 Imaging with NMR

Imaging with NMR is one of the most notable achievements of NMR. By adding a gradient to the external field \vec{B}_0 we create a coordinate dependency of the B_0 field, which implies a coordinate dependent ω_L . There are two different approaches to determine the density of the NMR-active material of the probe in 1 dimension.

The first method is called frequency coding, where one has a fixed gradient over time and measures the NMR signal in set times $t_n = N\Delta t$. Then one can do a discrete Fourier transform of the N measurements and gets a finite amount of $M_\perp(N\Delta z)$ for the different coordinates.

The second method is called phase coding, where one determines the phase of the precession all at a fixed time $t = t_0$ for different gradients. From that one gets a discrete amount of data points, with which one can do a discrete Fourier transform like in the first method.

The main difference between these two methods is the time needed to record data of N measurements. The first method requires $T_f = N \cdot \Delta t$ compared to the $T_\Phi = N \cdot t_1$ for the second method, where t_1 refers to the waiting time for probe relaxation between gradient changing.

For 2 dimensions a combination of both is used since with just 1 signal 2 coordinates should be determined. First a slice gets selected which is used to derive the positional information. Then the phase coding gradient is applied, afterwards the NMR signal is measured in steps of t_m . After finishing the frequency coding it changes the gradient, selects a slice again and does a phase coding again followed by a frequency coding. This process is repeated for N different gradients, taking $M\Delta t$ for each gradient. That leads to $N \times M$ data points which then can be transformed with a 2 dimensional Fourier transform into an image matrix of the object. One of the N cycles is illustrated in figure 3.

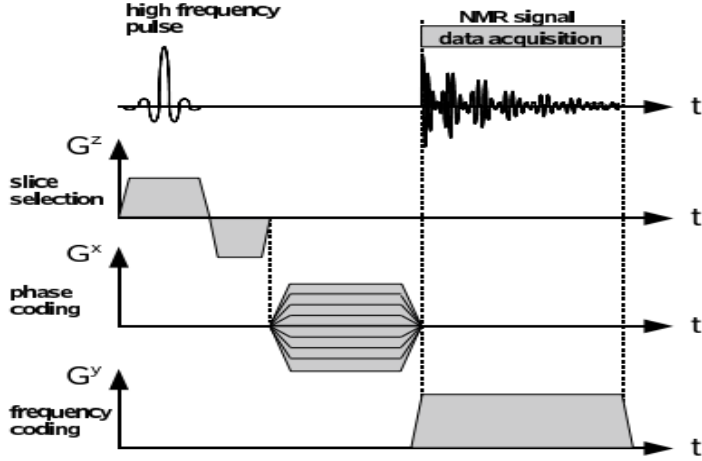


Figure 3: One of the N Loops needed for 2D Imaging taken from [2]

2 Layout of the experiment

2.1 Relaxation Time and Chemical Shift

For the first two parts of the this experiment we use a minispec p20 which produces both of the magnetic fields we need for the relaxation time and measuring the chemical shift.



Figure 4: The minispec p20, electronic unit on the left, magnetic unit on the right

The constant \vec{B}_0 , which is proportional to ω_L , can be adjusted by turning the screw sticking out of the Styrofoam as seen in Figure 4 . The ω_{HF} will be set by the electronic unit of the p20 seen on the left side of Figure 4. An oscilloscope is also provided to measure the characteristic time for a 90° pulse, which is needed to calibrate the electronic unit of the p20 for the relaxation time measurements. The tubes get inserted into the magnetic unit, parallel to the screw. A high-pressure air nozzle can be used to rotate the tube to ensure an evenly distributed density of the substance in the tube.

The data gets readout and analysed on a program written in Labview, the interface is shown in figure 5 via some example measurements.

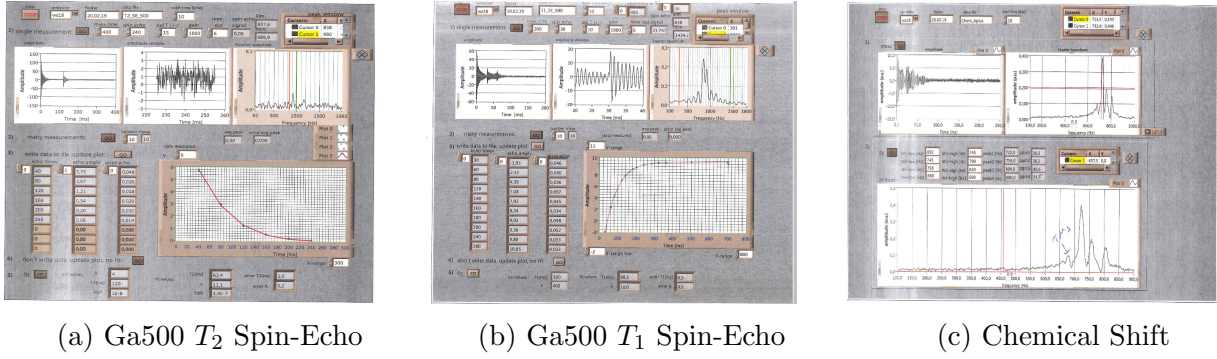


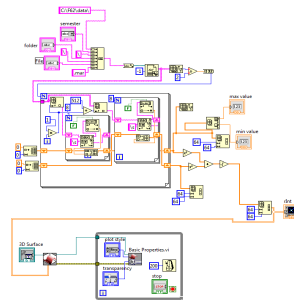
Figure 5: Example of the used Labviews

2.2 Imaging with NMR

We use a Bruker NMR analyzer 7.5 to generate the magnetic fields needed for 1D and 2D imaging. The readout gets fed into a computer where it gets analysed and can be later on displayed with a LabView .vi, examples of both can be seen in figure 6.



(a) the Bruker NMR analyzer mq7.5



(b) LabView .vi to display 2d image

Figure 6: The NMR analyzer and LabView for 2D imaging

3 Measurements and evaluation

3.1 Measurement of relaxation time

We measure T_1 and T_2 once with the spin echo method and T_2 again with the Carr-Purcell sequence for each Gd 500 and Gd 600.

probe	$T_{1,SE}$	$T_{2,CP}$	$T_{2,SE}$
Gd 500	68.1	66.1	62.4
Gd 600	99.2	84.0	78.6

Table 1: Summary of relaxation time measurements in ms

We can see 3 relations from these measurements: $T_1 > T_2$ and $T_{2,CP} > T_{2,SE}$ for both substances as well as $T_{600} > T_{500}$ for each different method.

The first can be explained by that T_2 contains additionally the effects of interactions of an ensemble of spins dephasing from each other.

The second relation can be explained by looking at the effects of the Carr-Purcell method. This method minimizes the effects of the molecular diffusion and field inhomogeneities, which

improves the precision of greater echo times.

The third relation can be attributed to the fact that the Gd 500 has higher concentration of Gd. The excitation energy of protons is dissipated in another way by interacting with Gd spins. Thus the more Gd there is, the shorter is the relaxation time.

From $\omega_L = 2\pi \cdot 19.8MHz$ we can calculate our external field \vec{B}_0 . And with the characteristic time $\Delta t = 1.29 \cdot 10^{-6}s$ for a 90° pulse we can calculate the solenoidal field \vec{B}_1 as well.

$$B_0 = \frac{\omega_L}{\gamma} = 0.48T \quad (15)$$

$$B_1 = \frac{\alpha}{\Delta t \gamma} = 4.3mT \quad (16)$$

with γ being the gyromagnetic factor mentioned in section 1.1.

3.2 Chemical shift

We measure the peaks and determine which peak is the TMS. After that we calculate the shift with the ppm, which is short for parts per million, given by the .vi and appoint them to a substance from figure 2b with the help of the provided reference sheet seen in figure 2a. The ppm to calculate the difference was read out of the .vi like in figure 5c.

	A+	B+	C+	D+	E+
$\Delta(2nd - TMS)$	2.2	2.1	2.0	3.9	2.6
$\Delta(3rd - TMS)$	3.9	6.9	11.6	6.3	7.5
$\Delta(4th - TMS)$	6.3				
Substance	fluoroacetone	p-xylol	acetic acid	fluoroacetonitril	toluol

Table 2: Summery of chemical shift in ppm

Even though the resonance frequency of Flour is much higher than the frequency we are using here, we can see the peaks caused by the Flour. They appear because of the spin-spin interaction between Flour and the proton (hydrogen) in FCH_2 , which leads to 2 different states for the electrons. For both D+ and A+ we can see each of these peaks at 3.9 and 6.3 on both spectra.

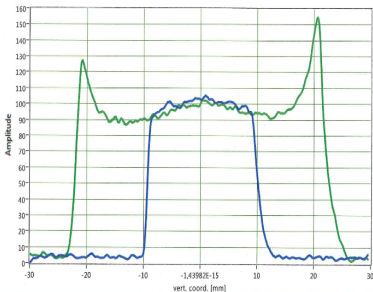
From the width of these peaks we can additionally calculate the energy resolution of this measurement as well, as the energy difference between the 2 different states FCH_2 can be in, depending on the spin-spin interaction of the electrons.

$$\Delta E_{res} = f_{FWHM} \cdot h = 19.9Hz \cdot 4.136eVs = 8 \cdot 10^{-14}eV \quad (17)$$

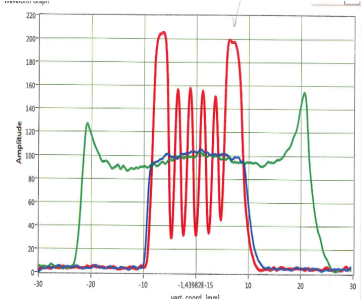
$$\Delta E_{dipole} = f_{\Delta F} \cdot h = 48Hz \cdot 4.136eVs = 2 \cdot 10^{-13}eV \quad (18)$$

3.3 Imaging with NMR

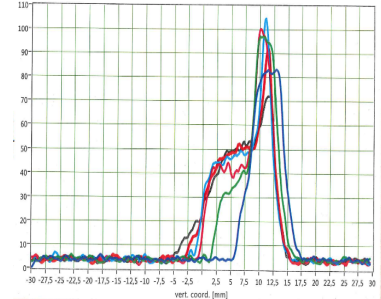
First we set the analyser in 1D mode. We poured 15 mL oil in a tube and could observe the capillary effect of the liquid on the glass of the tube. Then we added 35 mL oil, in total 50 mL, in the tube and we could see the boundaries of the analyser. They are caused by the



(a) 15 mL and 50 mL Oil



(b) Oil and Teflon (red graph)



(c) Oil on Sand over time

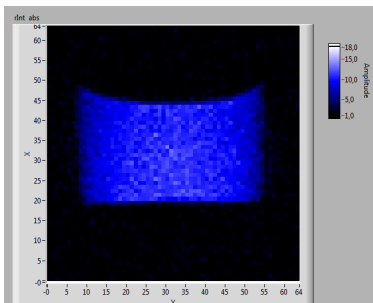
Figure 7: NMR imaging 1D

inhomogeneity of the magnetic field when probes are placed too far from the center of the coils. Both measurements can be seen in figure 7a.

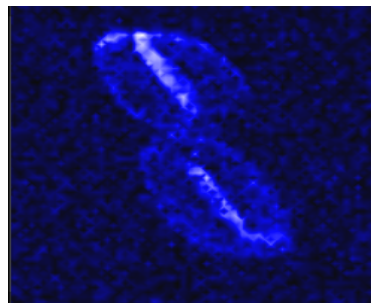
Then we put a teflon slice inside the oil tube and kept it partly immersed in oil. Dips on figure 7b show us that the Teflon layers aren't NMR-active.

Subsequently we filled an empty tube with 15 mm sand and 4 mm oil on top of it. We observed it in the analyser while the oil was seeping through the sand as shown in figure 7c. Though one might think that seeping of oil into sand could be compared to the diffusion of gas, the figure shows it is not the case, since it has seemingly random plateaus and drops in the seeping process.

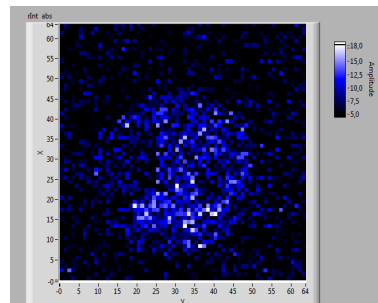
For the 2D imaging we inserted various objects into the analyser and displayed them with a LabView .vi. In figure 8 are some of the images we made.



(a) 15 ml Oil 2D



(b) Peanuts in Shell



(c) A Cherry Tomato

Figure 8: NMR imaging 2D

Figure 8a is the 15 mL oil tube used for figure 7a being imaged in 2D. One can still see the capillary effect on the edges of the tube.

In figure 8b a peanut is imaged. The white stripes between the two halves of a single nut is the air between the two halves. All of this can be observed without even opening the shell, which illustrates the power of this technique.

Finally we took a picture of horizontal slice of a cherry tomato, as shown in figure 8c. Since the cherry tomato contains and is mainly consists of water, which is not NMR-active, it's difficult to differentiate the signal of object itself and its surrounding noise, and hence the image only shows a blurry shape.

4 Discussion

The fits from the .vi program gave us errors of fit parameters for T_2 of around 2%, but the difference between relaxation time measured by spin-echo and by Carr-Purcell method is around 7%. In that sense we can see that molecular diffusion and inhomogeneities of magnetic field are major sources of systematic errors. And since it's still hard to estimate their effects in Carr-Purcell method, also it should be considered that some of the measurements had very few data points, it leads to the question how convincing such a fit error would be.

For p-xylol and toluol, in the substances determination by chemical shift, we expected the same peak positions with different amplitude, since they have similar NMR-active components. But as seen in table 2, toluol's peak experienced a relative large shift compared to the other substances. For example the peak for CH_3 for p-xylol and acetic acid appear both around 2.0, but at 2.6 for toluol. The same could also be observed for the 3rd peaks, the benzol.

Unlike other spectroscopic techniques, NMR is unaffected by sample color and surface properties. Hence it is perfectly suited for many fields, e.g. food industry, healthcare industry etc., because it is a non destructive and non-invasive measurement that requires no sample preparation [1].

Although in this experiment we use NMR to differentiate several substances, in reality it is in some cases not practical. Since, as shown in figure 2a, particular peaks can be referred as several parts and as long as one doesn't already have a general idea about the substance, it can be near impossible to find out what substance one are dealing with alone off those resonances.

Some modern applications of NMR are for example the spectroscopy of ^{31}P , which is an essential part of living cells, and Magnetic Resonance Imaging (MRI), which is widely used for medical purposes in modern day and age.

References

- [1] *Manual pf the minispec mq series.* URL: https://www.bruker.com/fileadmin/user_upload/8-PDF-Docs/MagneticResonance/TD-NMR/minispec_mqseries_T137089.pdf.
- [2] R. Schicker. *Nuclear Magnetic Resonance F61/F62.* 2.0. was used for most of this reports content. Physikalisches Institut. Philosophenweg 12, 69120 Heidelberg, Apr. 14, 2010.